Springer

KSME

Journal of Mechanical Science and Technology 32 (2) (2018) 659~670
www.springerlink.com/content/1738-494x(Print)/1976-3824(Online)
DOI 10.1007/s12206-018-0113-5

Nanofluid (H_2O-Al_2O_3/CuO) flow over a heated square cylinder near a wall under the incident of Couette flow †

Swati Sharma[1], Dilip K. Maiti[2,*], Md. Mahbub Alam[3] and Bhupendra K. Sharma[1]

[1]*Department of Mathematics, Birla Institute of Technology and Science, Pilani - 333031, RJ, India*
[2]*Department of Applied Mathematics with Oceanology and Computer Programming, Vidyasagar University, Midnapur - 721102, WB, India*
[3]*Institute for Turbulence-Noise-Vibration Interaction and Control, Shenzhen Graduate School, Harbin Institute of Technology, Shenzhen, China*

(Manuscript Received March 10, 2017; Revised August 30, 2017; Accepted November 13, 2017)

Abstract

A long heated cylinder was placed near a cold wall under the incident of a Couette flow. The conventional fluid was chosen as water *(H_2O)*. The nanoparticle materials were selected as Al_2O_3 and CuO. The governing Navier-Stokes and energy equations were solved numerically through a finite volume method on a staggered grid system using QUICK scheme for convective terms and SIMPLE algorithm. The dependencies of hydrodynamic and heat transfer characteristics of the cylinder on non-dimensional parameters governing the nanofluids (Particle concentrations (φ), diameter (d_{np}), and particle materials) and the fluid flow (Peclet number *Pe* and gap height ratio *L)* were explored here. The shifting of the front stagnation point due to the addition of nanoparticles in the base fluid was investigated. A comparison between the heat transfer enhancement (Nu_M) of the cylinder and its drag coefficient's (C_D) increment/reduction was made by presenting their ratio Nu_M/C_D. The least square method was applied to the numerical results to propose $Nu_M = Nu_M(Pe)$ and $Nu_M = Nu_M(L)$.

Keywords: FVM; Heat transfer enhancement; Nanofluid; Heated square cylinder; Gap height

1. Introduction

The study of the flow past bluff bodies has been imperative for a long time, because of the intrinsic complexities and importance of the flow in many practical applications such as nuclear reactor fuel rods, drying of different materials, cooling of glass, plastics and industrial devices, and chemical reactors. As such, heat transfer characteristics of the flow over bluff bodies have been examined in the literature. The flow field and various transport coefficients strongly depend on the shape and configuration of various bluff bodies including circular cylinders, flat plates, and other blunt cross-sections. Recently, square cylinders have received renewed attention because of their relevance to enhance the cooling from electronics devices. Yang and Fu [1] studied the unsteady heat transfer from a heated electronic component subjected to a flow. It is more difficult to understand when these bluff bodies are placed in the proximity of a wall. Apart from these applications, this issue is classical in advanced fluid mechanics and heat transfer.

The challenges in enhancing the heat transfer rate in the above applications have attracted the attention of the fluid dynamics community. Nanoscale particle (< 100 nm) suspensions in base fluids such as water, ethylene glycol or oil (Nanofluids) have often been used as an alternative heat transfer medium due to superior thermal properties (Choi [2]). These fluids can constitute very interesting alternatives for electronic liquid cooling applications (Nguyen et al. [3]), automotive sector, nuclear reactors, computers and X-rays (Azmi et al. [4], Kakac and Pramuanjaroenkij [5]). Several effective parameters on the thermal conductivity of nanofluids have been presented, such as nanofluid temperature, concentration φ (Murshed et al. [6]) and materials (Murshed et al. [6]). Furthermore, some researchers believe that the Brownian motion of nanoparticles inside the fluid is a key mechanism of heat transfer in nanofluids (Ebrahimnia-Bajestan et al. [7]).

Sharma and Eswaran [8] focused on the heat transfer characteristic around a square cylinder for uniform heat flux and constant cylinder temperature. The flow and heat transfer past a heated cylinder mounted horizontally above a plane wall was studied by Bhattacharyya et al. [9]. Dhinakaran [10] performed a numerical simulation for the heat transfer from a square cylinder near a moving wall.

Zeinali et al. [11] indicated that the H_2O-Al_2O_3 nanofluid

*Corresponding author. Tel.: +91 3222276554 (Extn. 452), Fax.: +91 3222275329
E-mail address: d_iitkgp@yahoo.com
† Recommended by Associate Editor Jungil Lee

causes a greater enhancement in heat transfer coefficient compared with H_2O-CuO. Valipour et al. [12] investigated the fluid flow and forced convective heat transfer around a square obstacle utilizing H_2O-Al_2O_3 nanofluid at low Reynolds numbers. Ebrahimnia-Bajestan et al. [7] concluded that increasing φ enhances the heat transfer. Bovand et al. [13] showed that time average Nusselt number increases by using nanoparticles and increases ϕ. The heat transfer increases by considering the Brownian effects compared with that without Brownian motion. A numerical study on MHD natural convection for alumina-water nanofluid within the circular cylindrical enclosure with an inner triangular was performed by Sheikholeslami et al. [14]. Salimpour and Dehshiri [15] experimentally investigated the laminar forced convective heat transfer of TiO_2/water nanofluids through conduits with different cross sections.

Heidary and Kermani [16] showed that the heat transfer in channels can be enhanced up to 60 % due to the presence of nanoparticles and the blocks in channels. Azimi and Riazi [17] analyzed the heat transfer and nanofluid flow between two non-parallel walls for both converging/diverging cases. Etminan-Farooji et al. [18] showed that for any given d_{np} there is an optimum value of φ that results in the highest heat transfer coefficient. Sarkar and Ganguly [19] demonstrated entropy generation due to laminar mixed convection of nanofluid past a square cylinder in vertically upward flow with the range of φ: 0-20 %.

For cavity flow, Alloui et al. [20] studied natural convection of nanofluids and various models for calculating the effective viscosity and thermal conductivity of nanofluids. Noghrehabadi et al. [21] showed an improvement in heat transfer rate for the whole range of Rayleigh numbers when Brownian and thermophoresis effects are considered. Malik and Nayak [22] numerically studied mixed convection flows of nanofluid in a lid-driven cavity.

To our knowledge, there is no literature on the nanofluid flow and heat transfer around a heated square cylinder near a wall. The presence of nanoparticles (Al_2O_3/CuO) in the flowing base fluid (Water) would enhance the heat transfer from the heated cylinder. The presence of shear in the flow and the wall confinement produces an asymmetry in the two separated shear layers emerging from the upper and lower faces of the cylinder. The present study deals with the heat transfer performance of the nanofluids flowing over a heated square cylinder near a wall by varying the parameters governing the fluid flow: Peclet number *(Pe)* and gap height ratio (L), governing the nanofluids: Particle materials (Al_2O_3/CuO), concentration (φ) and diameter (d_{np}) of materials. Explicit forms of $Nu_M = Nu_M(Pe)$ *and* $Nu_M = Nu_M(L)$ are proposed using least square method.

2. Methodology

2.1 Problem formulation and governing equations

A long square cylinder (with height A) maintained at a constant temperature T_W was placed parallel to the wall lying along the x*-axis at a gap height H (See Fig. 1). The ambient stream has a uniform temperature T_0 (< T_W). The inlet flow is taken as the Couette flow based linear velocity profile, which is in accord with the boundary layer theory (Maiti [23]).

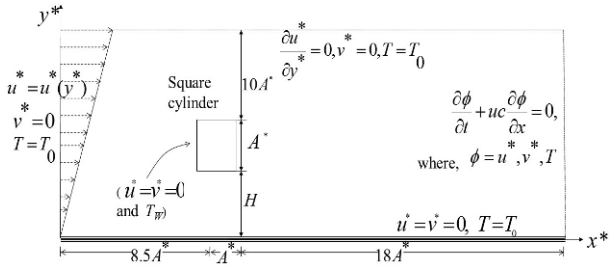

Fig. 1. Schematic of flow configuration.

There are two approaches (Single-phase or two-phase model: Akbari et al. [24], Corcione et al. [25] and Vanaki et al. [26]) for numerical simulation of nanofluid flow problem. Akbari et al. [24] reported that single- and two-phase models predict almost identical hydrodynamic fields but the two-phase model gives closer predictions of the convective heat transfer coefficient to the experimental data; nevertheless, the two-phase model over-predicts the enhancement of heat transfer. Corcione et al. [25] and Vanaki et al. [26] observed that nanofluids behave more like single-phase fluids than conventional solid–liquid mixtures. Vanaki et al. [26] confirmed that two-phase modeling renders a higher value of heat transfer coefficient than the homogeneous modeling, but because of contradictory results among the recently conducted numerical works, it is still controversial whether the two-phase approach gives credible results. To the best of the authors' knowledge, almost all the available studies on the nanofluid flow over circular/triangular/square cylinders are based on a single-phase modeling approach. Moreover, a single-phase model is simpler to implement and requires less computational time, and therefore it is adopted here.

The flow is considered to be two-dimensional and laminar. The dimensional Navier-Stokes equations along with the energy equation governing the nanofluid flow are given by:

$$\nabla \cdot V^* = 0 \tag{1}$$

$$\frac{\partial V^*}{\partial t^*} + (V^* \cdot \nabla)V^* = -\frac{1}{\rho_{nf}}\nabla p^* + \nu_{nf}\nabla^2 V^* \tag{2}$$

$$\frac{\partial T}{\partial t^*} + (V^* \cdot \nabla)T = \alpha_{nf}\nabla^2 T\,. \tag{3}$$

Here V^*, p^* and t^* denote the dimensional velocity vector, pressure and time, respectively, while ρ_{nf}, ν_{nf} and α_{nf} denote density, kinematic viscosity and thermal diffusivity of the nanofluid, respectively. The incident velocity profile at the surface multiplied by A leaving $U_0 = \lambda A$ is taken as the velocity scale. The height of the cylinder A and temperature difference $\Delta T = T_W - T_0$ are considered as the characteristic

length and temperature scales, respectively.

The nanofluid flow field is characterized by the non-dimensional parameters: Gap height *L,* Prandtl number *Pr,* Reynolds number *Re*, and Peclet number *Pe* which are defined, respectively by

$$L=\frac{H}{A},\ \mathrm{Pr}=\frac{\nu_{nf}}{\alpha_{nf}},\ \mathrm{Re}=\frac{U_0 A}{\nu_{nf}},\ Pe=\mathrm{Re}^{*}\mathrm{Pr}. \tag{4}$$

At the plane wall and cylinder surface, the no-slip boundary condition is applied. At the far upstream, Couette flow based linear velocity profile $u^{*}=U_0 y^{*}/A$ is considered. The mathematical form of the boundary conditions used in this study to solve the above equations is shown in the computational domain (Fig. 1).

The flow is assumed to start impulsively at a particular value of *Re*. The converging solution (after the transient state) computed at this *Re* is considered an initial solution for the case of other values (Lower/higher) of *Re.* A time-independent stable numerical solution is achieved by advancing the flow field variables through a sequence of short time steps of duration Δt.

The local Nusselt number (*Nu*), face-wise average Nusselt number *(Nu_{avg})* and mean Nusselt number (Nu_M) of the cylinder are defined as

$$Nu=\frac{hA}{\kappa_{nf}},\qquad Nu_{avg}=\frac{1}{A}\int_0^A (Nu)dl\ \ \&$$
$$Nu_M=\frac{1}{4}\sum_{AB} Nu_{avg},\ \ \text{respectively} \tag{5}$$

where h and k_{nf} are convective heat transfer coefficient and thermal conductivity of nanofluid, respectively.

2.2 Nanofluid modelling

Water *(H_2O)* is considered as the base fluid. The nanoparticles are assumed to be of uniform shape and size. In addition, it is assumed that the nanoparticles are homogeneously distributed in the base fluid. The thermophysical properties of the nanofluids are assumed constant. The material of the nanoparticles is selected as Al_2O_3 and CuO. Thermophysical properties are calculated as follows:

Density: The density of nanofluids is calculated from the proposed equation of Pak and Cho [27].

Specific heat: The specific heat of nanofluids is determined using the equation given by Xuan and Roetzel [28] that assumes thermal equilibrium between the base fluid and the nanoparticles.

Thermal conductivity: The relation proposed by Koo and Kleinstreuer [29] and later modified by Vajjha and Das [30] for thermal conductivity as a two terms function (Which takes into account the effect of $d_{np,}$ φ, temperature T and the properties of the base fluid) is considered here. Kim et al. [31] experimentally, and Ebrahimnia Bajestan et al. [7] numerically, confirmed that this model predicts the thermal conductivity and hence the heat transfer coefficient of nanofluids more accurately as compared to the models based on the pure static conditions of the nanofluids.

Viscosity: Masoumi et al. [32] developed a theoretical model for the prediction of the effective viscosity of nanofluids, and this takes care of Brownian motion, temperature of the base fluid, d_{np}, ϕ, nanoparticle density and base fluid physical properties. The model is as follows:

$$\mu_{nf}=\mu_{bf}+\frac{\rho_{np} V_B d_{np}}{72C\delta} \tag{6}$$

where, $V_B=\frac{1}{d_{np}}\sqrt{\frac{18k_bT}{\pi\rho_{np}d_{np}}}$ is the Brownian velocity, C is the correlation factor defined by

$$C=\mu_{bf}^{-1}[a\varphi+b] \tag{7}$$

with

$$a=-1.133\times10^{-6}\times d_{np}\times10^{9}-2.771\times10^{-6}$$
$$b=90\times10^{-8}\times d_{np}\times10^{9}-3.93\times10^{-7}, \tag{8}$$

and $\delta=\left(\frac{\pi}{6\phi}\right)^{1/3} d_{np}$ is the distance between the centres of particles. It may be noted that the factor of 10^9 is multiplied to d_{np} in order to convert to meter.

Thermophysical properties of water (ρ_{np}, $C_{p,bf}$, k_{bf} and μ_{bf}) are calculated at fluid temperature 300 K from the relations given in Etminan-Farooji et al. [18]. Physical properties of nanoparticles (ρ_{np}, $C_{p,np}$ and k_{np}) are taken from Etminan-Farooji et al. [18].

2.3 Numerical method

The pressure correction based iterative algorithm SIMPLE based on Finite volume method (FVM) with staggered grids, is applied here. A third-order accurate QUICK (Quadratic upstream interpolation for convective kinematics) is employed to discretize the convective terms and central differencing for diffusion terms. The numerical methodology (Staggered grid, FVM, QUICK and SIMPLE algorithms) used here has been discussed in the previous study (Bhattacharyya et al. [9]).

2.3.1 Size of computational domain and consideration of grid

The height of the top lateral boundary and the inflow boundary are chosen to be large enough so that the influence of the boundary conditions on the wall shear stress is very weak. The inflow, outflow and top lateral boundary distances

Table 1. Grid refinement study on Nu_M, C_D and C_L for the case of H_2O-CuO nanofluid at Pe = 200 for different d_{np} and ϕ.

d_{np}(φ)	Re	Pr	Grid	Nu_{avg}	C_L	C_D
30 nm (2 %)	35.4	5.650	550 × 475	7.17	1.77	4.09
			800 × 600	7.24	1.77	4.1
			196 × 140	6.81	1.71	3.94
30 nm (4 %)	33.3	6.001	550 × 475	7.55	1.83	4.17
			800 × 600	7.6	1.84	4.18
			196 × 140	7.25	1.78	4.03
100 nm (2 %)	40.6	4.930	550 × 475	7.15	1.63	3.93
			800 × 600	7.2	1.63	3.94
			196 × 140	6.68	1.57	3.77
100 nm (4 %)	46.0	4.348	550 × 475	7.7	1.51	3.79
			800 × 600	7.75	1.51	3.8
			196 × 140	7.33	1.46	3.65

are noted in Fig. 1. Further changes on the boundary distances do not produce any significant changes in the results. The errors due to computational domain size and boundary conditions can be regarded as very small (within a few percent).

A non-uniform grid distribution is considered for distributing uniform grids along the surfaces of the cylinder with expansion factors for the far-fields (Away from the surfaces) starting with δ_1 = 0.004, the first grid point away from the body. A non-uniform grid of size 550 × 475 with the first and the second number being the number of mesh points in the *x*- and *y*- directions, respectively, is considered in the computational domain. To see the effect of grid sizes on the hydrodynamic and heat transfer characteristics due to the variation of parameters governing the nanofluid, Table 1 was prepared by varying the grid between 196 × 140 to 800 × 600 for φ = 2 & 4 %, d_{np} = 30 & 100 nm at Pe = 200. The results of 550 × 475 were compared with those of 800 × 600 and 196 × 140, and accordingly the relative percentage error was calculated. It is observed from Table 1 that the major differences of these hydrodynamic and heat transfer characteristics occur on the very coarse grid, while the differences of these characteristics are found minor between 550 × 475 and 800 × 600. So, the error is tending to zero with the increase in the number of grids. Note that the computation based on the finer grid takes much more time than that on medium grids. Therefore the medium grid 550 × 475 was considered as a reasonably fine for the calculation domain.

2.3.2 Validation of numerical code

The numerical code used in the previous studies (e.g., Bhattacharyya and Maiti [34] for a single square cylinder, Maiti [23] for a single rectangular cylinder and Bhattacharyya et al. [9] for a square heated cylinder near a wall) was used here. The previously published results of the present authors also show the validity of the used code for this work. The numerical code for the present case of heat transfer, also validated with Sharma and Eswaran [8], are presented in Table 2 for the cases of the uniformly heated cylinder and cylinder with constant heat flux. The table shows an excellent match between the two results in Nu_M and St computations.

Table 2. Comparison of present Nu_M and St with that obtained by Sharma and Eswaran [8]. Here $S \rightarrow$ Sharma and Eswaran [8] results, $P \rightarrow$ Present results.

		Constant temperature				Uniform Heat Flux			
		B/H = 20 %		B/H = 50 %		B/H = 10 %		B/H = 20 %	
Re		P	S	P	S	P	S	P	S
50	*St*	-	-	-	-	0.18	0.18	-	-
	Nu_M	3.49	3.57	4.84	4.93	3.81	3.82	3.93	3.94
100	*St*	0.24	0.25	0.51	0.53	0.22	0.22	0.246	0.24
	Nu_M	4.57	4.67	6.4	6.44	5.04	5.03	5.03	5.05
150	*St*	0.21	0.21	0.51	0.53	0.2	0.19	0.2	0.19
	Nu_M	5.5	5.53	7.41	7.47	5.89	5.89	5.82	5.81

The code was also validated for the case of nanofluid modelling. The computed heat transfer coefficient (*h*) was compared with that obtained by Etminan-Farooji et al. [18]. The comparison is presented in Table 3. As can be seen, the maximum percentage difference of *h* of the present calculation from those of Etminan-Farooji et al. [18] is 4.59 %. Relative percentage error was around 1 % in most of the cases. The results show the excellent agreement of the present result over the whole range of *Pe*.

3. Results and discussion

The numerical experiments were made with the choice of following parameter values:

Diameter (d_{np}): 30 nm, 50 nm and 100 nm.

Concentration (φ): 2 %, 4 % and 6 %. Masoumi et al. [32] mentioned that Eq. (7) is valid for φ < -*b*/*a*, where a and b are defined in Eq. (9). In the present calculation the values of d_{np} were taken as 30, 50 and 100 nm, accordingly -*b*/*a* value registers 6.276, 6.912 and 7.415 %, respectively. Therefore, the value of φ can be considered up to 6 %. The variations of k_{nf}/k_{bf} and μ_{nf}/μ_{bf} with φ for d_{np} = 30, 50 & 100 nm are plotted in Fig. 2. As seen, both ratios increase with φ. An anomaly behavior of μ_{nf} with φ while changing φ from 5 to 6 % for the case of d_{np} = 30 nm may be noted here.

Peclet number (Pe): Pe = 25, 50, 100, 150, 200, 300 and 400.

Prandtl number (Pr): *Pr* is defined based on the nanofluid characteristics, different for different values of d_{np} and φ as well as materials. *Pr* is ranged in 4.414 - 19.86.

Reynolds number (Re): For a particular fluid (Fix *Pr*), *Pe* variation results in the variation of *Re* (= 13-96.6). Here the flow was steady for all the cases since the critical *Re* at which the cylinder placed at a gap height 0.5*A* sheds vortices is 125 (Bhattacharya and Maiti [34]).

Gap height L : 0.1, 0.25, 0.5, 1.0, 1.5, 2.0, 3.0 and 4.0.

Table 3. Comparison of present heat transfer coefficient (h) with that obtained by Etminan – Farooji et al. [18]. Here $EF \rightarrow$ Etminan- Farroji et al. [18] results, $P \rightarrow$ Present results, $E \rightarrow EG{:}W$, $W \rightarrow$ Water.

Nanofluid	Pe = 25		Pe = 50		Pe = 100		Pe = 200	
	EF	*P*	*EF*	*P*	*EF*	*P*	*EF*	*P*
Al_2O_3, 2 %, 30 nm^W	1.59	1.56	2.1	2.05	2.8	2.7	3.85	3.72
Al_2O_3, 4 %, 30 nm^W	1.67	1.67	2.2	2.17	2.92	2.86	4.1	3.92
CuO, 2 %, 30 nm^W	1.6	1.57	2.17	2.07	2.75	2.71	3.8	3.7
CuO, 4 %, 30 nm^W	1.68	1.73	2.27	2.25	3.0	2.97	4.01	3.9
CuO, 2 %, 100 nm^W	1.57	1.53	2.05	1.99	2.71	2.64	3.7	3.57
Al_2O_3, 2 %, 30 nm^E	0.89	0.9	1.13	1.11	1.49	1.43	1.9	1.86
Al_2O_3, 4 %, 30 nm^E	0.93	0.94	1.19	1.18	1.56	1.52	2.01	1.97
Al_2O_3, 2 %, 100 nm^E	0.85	0.83	1.09	1.04	1.4	1.36	1.82	1.77
Al_2O_3, 4 %, 100 nm^E	0.89	0.92	1.15	1.17	1.52	1.49	2.02	1.95
CuO, 2 %, 30 nm^E	0.89	0.9	1.12	1.11	1.41	1.42	1.97	1.9
CuO, 4 %, 30 nm^E	0.94	0.96	1.21	1.22	1.58	1.56	2.14	2.05
CuO, 2 %, 100 nm^E	0.85	0.82	1.1	1.06	1.4	1.37	1.82	1.78
CuO, 4 %, 100 nm^E	0.9	0.92	1.17	1.19	1.55	1.52	2.01	2.0

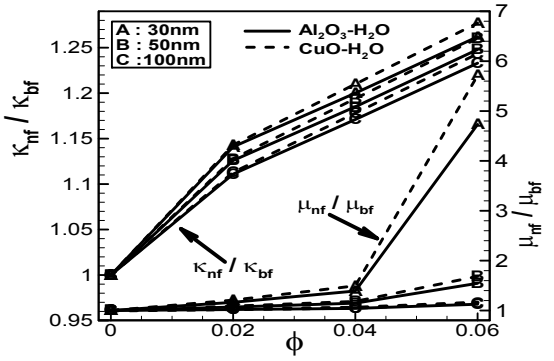

Fig. 2. Ratio of thermal conductivity and viscosity of both the nanofluids (H_2O-CuO and H_2O-Al_2O_3) at different d_{np} and ϕ.

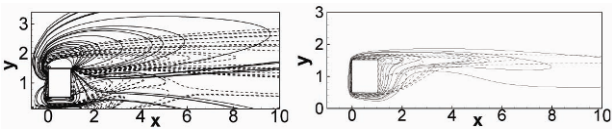

(a) (b)

Fig. 3. (a) Vorticity contours; (b) isotherms around the heated square cylinder of H_2O-CuO nanofluid with ϕ = 4% and d_{np} = 30 nm at Pe = 25 (Solid line) and Pe = 400 (Dashed line) for L = 0.5.

3.1 Overview of flow and temperature field

Numerical flow visualization for H_2O-CuO nanofluid with d_{np} = 30 *nm* and φ = 4 % at Pe = 25 (Solid line) and 400 (Dashed line) in Fig. 3(a) for L = 0.5 suggests that there is no shedding of vortex/vortices from the cylinder, and the flow is found to be completely steady since Re = 4.1 is much smaller than the critical Re = 125. Lower shear layer of the cylinder occupies most of the surface of the cylinder and upper shear layer of the cylinder lies only on top of the cylinder. With the increase of Pe (*i.e.,* Increase of Re for fixed nanofluid) the

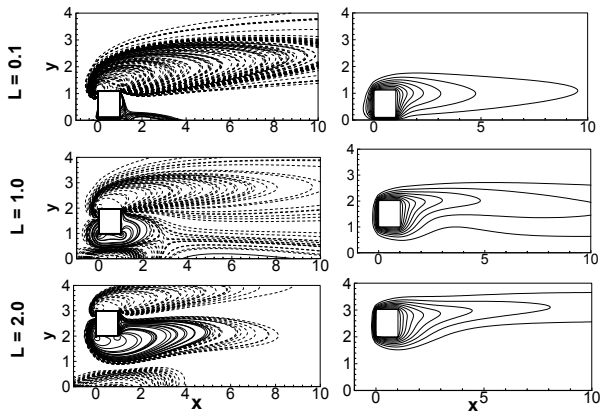

Fig. 4. Vorticity contours (Left side) and corresponding isotherms lines (Right side) of H_2O-CuO nanofluid with ϕ = 4 % and d_{np} =50 nm at Pe = 25. In vorticity contours (Left side), solid lines: Positive vorticity and dashed lines: Negative vorticity.

lower shear layer is slightly detached from the rear face and the upper shear layer is convected downstream without shedding. The layers of the cylinder are not interacting with each other. Only a weak interaction between the wall shear layer and cylinder's lower shear layer takes place. The effect of gap height on the flow field is discussed based on the vorticity contour presented in Fig. 4(a) at Pe = 25 with d_{np} = 50 nm and φ = 4 %. For a gap height larger than 0.5, the above interaction between the cylinder and wall diminishes and at L = 2.0, no more interaction is observed and the lower shear layer of the cylinder takes its proper form. However, at a lower L = 0.1, the lower shear layer of the cylinder is almost vanished due to a very negligible flow through the gap (Fig. 6(b)). Though the increment of the gap height is mechanically similar to that of Re, the flow is found to be steady even at L = 4.0 (Not presented here). The effect of concentration (φ) on the vorticity

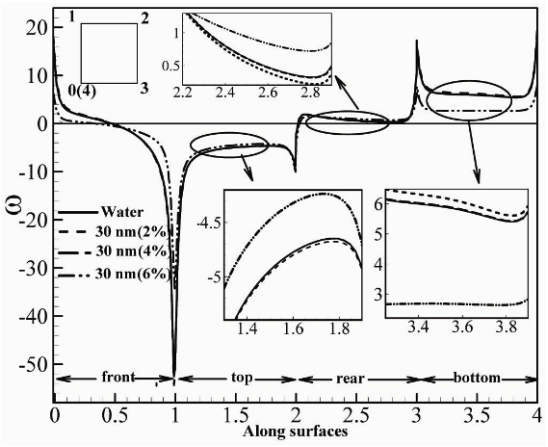

(a)

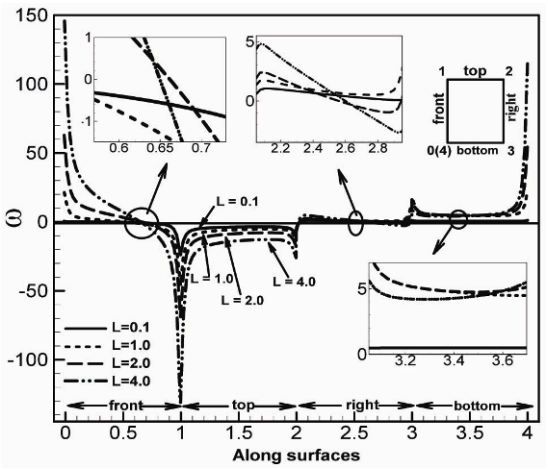

(b)

Fig. 5. Wall vorticity (ω) distribution around the cylinder for H_2O-CuO nanofluids for (a) different ϕ at dnp = 30 nm, Pe = 100 and L = 0.5; (b) different L with ϕ = 4 %, d_{np} = 50 nm and Pe = 25.

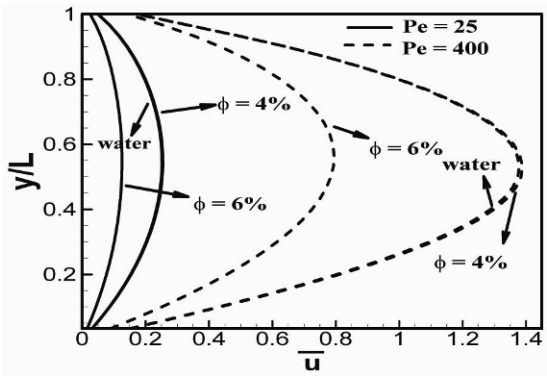

(a)

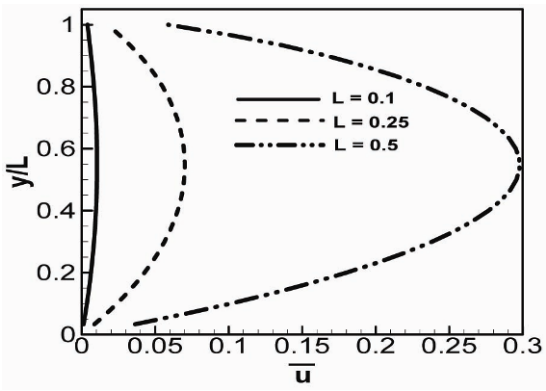

(b)

Fig. 6. Horizontal velocity profile along the vertical direction (y) at the exist position (x*=a) of the gap between the cylinder's lower face and the wall for (a) different Pe and ϕ at d_{np}= 30 nm and L = 0.5; (b) different L with d_{np}= 50 nm, ϕ = 4 % at Pe = 25.

generated at the cylinder surfaces is exemplified in Fig. 5(a) for H_2O-CuO nanofluid. As seen the wall vorticity (ω) decreases sharply from the front-bottom corner (Point 0) and reaches to minimum value (First minima) at the point 1. Thereafter, it rapidly increases along the top face and remains almost steady in most part of the top face, followed by sudden decrease at the end of this face providing its second minima. Again it starts increasing to reach a constant (Close to zero-value) on the rear face, and then reaches to a second maxima (First maxima being at the point 0) at the point 3. Finally, after a sudden decrease, it maintains a constant positive value (Depending on φ value) and then reaches a third maximum at the point 4. Overall, the sharpest variation in ω can be seen at the front-top corner, pointing to a large variation in the velocity. The global minimum and maximum of ω register at the point 1 and point 0, respectively. From the variation of ω on the front face, it may be deduced that velocity variation along this face is less for φ = 6 % than that for φ = 0-4 %. Front stagnation is shifted very close to the bottom of the front face for the case of φ = 6 %. From a closer view of top, rear and bottom faces, the effect of φ on the negativity/positivity in ω around the top/bottom face is negligible while changing φ from 0 to 4; however, the numerical value of ω on these faces decreases with increase in φ from 4 to 6 %. These observations on the wall vorticity can be justified from the increased viscosity of the nanofluid. The effect of gap height (L) on ω can be seen in Fig. 5(b). As seen, the magnitude of ω is directly proportional to L since the increase of L is equivalent to expose the cylinder to higher velocity region under the present flow condition. A change of sign of ω on the rear face at a higher L may be noted here. The front stagnation point moves towards the bottom side as the cylinder moves close to the plane wall. A similar effort was made for H_2O-Al_2O_3 nanofluid, not presented here, and the effect of nanoparticle material (Al_2O_3, CuO) on the vorticity around the cylinder surfaces is almost negligible.

As seen in Fig. 6, the gap flow (between the cylinder's lower face and the wall) becomes stronger with the increase of Pe and/or L and the velocity overshoots (Jet action). Velocity profile takes its parabolic form in the gap flow. When the contour is very close to the wall (Fig. 4(a)), the gap flow is found almost stagnant. Therefore, the heat transfer from the cylin-

der's lower face is expected to be more for the case of the presence of the wall, in comparison to that of the absence of the wall. It is evident from Fig. 6(a) that because of high viscosity at φ = 6 %, the flow becomes slower in comparison to the counterpart in φ = 0-4 %.

As both vorticity and thermal energy are being transported by the flow in the wake, the contour lines of vorticity and temperature have similar features (Figs. 3 and 4). Moreover, the equation of temperature is similar to that of vorticity. The temperature distributions show that the heat is distributed within the flow field as isolated warm blobs. These warm blobs are captured within the vortex structures and advected downstream without being influenced too much by mixing with their surroundings. The thermal boundary layer growth starts almost symmetrically from the front face of the cylinder and becomes thicker toward the rear. A higher induced temperature gradient in the vicinity of the cylinder surface is visible from the contours. Except for L = 0.1 in Fig. 4, the thermal boundary layer on the front surface is thinner and produces a higher heat transfer compared to the other surfaces. Temperature contours are clustered near the front top and bottom corners, indicating that convective cooling of the cylinder is maximum in these regions, while the convective cooling along the rear face is expected to be low. This is because of the circulation generated behind the cylinder, *i.e.,* counter-rotating cell sweeps the heated fluid away from the wall at a lower rate. Apparently, the thickness of thermal boundary is reduced at a higher *Pe* and *L*. At lower L = 0.1, the hot cylinder is very close to the cold wall, as a result conductive heat transfer through the wall is expected to occur, indicating higher heat transfer from the bottom of the cylinder.

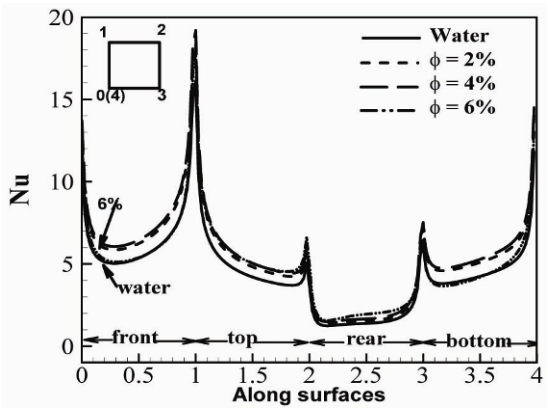

(a)

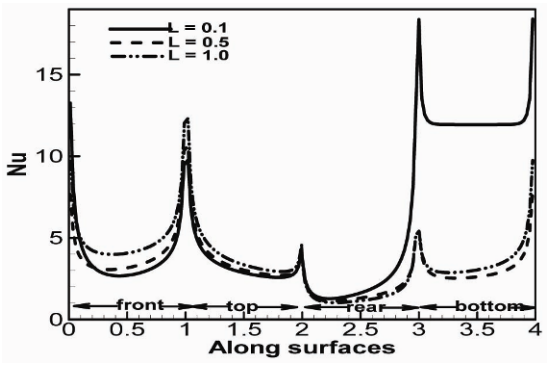

(b)

Fig. 7. Local Nusselt number (*Nu*) distribution around the heated cylinder for H_2O-Al_2O_3 nanofluids for (a) different φ at d_{np} = 30 nm and *Pe* = 100 and L = 0.5; (b) different L with φ = 4 %, d_{np} = 50 nm and *Pe* = 25.

3.2 Temperature distribution, hydrodynamic and heat transfer characteristics

Fig. 7 plots the local Nusselt number (*Nu*) distribution around the cylinder surfaces for H_2O-Al_2O_3 nanofluid for different φ (Fig. 7(a) at d_{np} = 30 *nm*, *Pe* = 100 and L = 0.5*)* and L (Fig. 7(b) at d_{np} = 50 nm, φ = 4 % and *Pe* = 25). *Nu* attains local maxima at the four corners of the cylinder since the thermal boundary layer at these points is thinnest, having a higher thermal gradient. As seen in Fig. 7(a), the front face has a larger heat transfer rate compared to other faces as the incoming cold fluid directly impacts on it. The variation of *Nu* along the rear face is almost constant since the originating weak vortex rotates on this surface without being shed (Fig. 3). Apparently, the *Nu* distributions around the top (Faces 1-2) and bottom (Faces 4-3) faces are not in symmetry since the incident flow is not symmetric. The heat transfer from the cylinder is clearly enhanced due to the addition of nanoparticles in the base fluid (Water) and *Nu* increases with φ for φ = 2 % to 4 %. The addition of nanoparticles is more effective on the front and bottom faces of the cylinder. Surprisingly, heat transfer is found to decrease with the increase of φ from 4 % to 6 % and the *Nu*-distribution at φ = 6 % is close to that without nanoparticles. The increase of ϕ in the base fluid enhances the μ_{nf} as well as κ_{nf}. It is plausible that the role of thermal conductivity on the heat transfer is opposite to that of viscosity. As observed in Fig. 2, the viscosity at this d_{np} is highly sensitive to φ while changing φ from 4 % to 6 %. The rate of increment for thermal conductivity is around 1.05 for both cases: φ = 2 % to 4 % and 4 % to 6 %, while this rate for viscosity is 1.195 and 3.40 for φ = 2 % to 4 % and 4 % to 6 %, respectively (Fig. 2). Therefore, it shows that for the case of φ = 4 % to 6 % at d_{np} = 30 *nm*, Nusselt number increases nominally due to the increase in κ_{nf}, while decreases marginally due to the μ_{nf} (by reducing the speed of incident velocity). It is observed from Fig. 7(b) that Nu-distributions at different L are qualitatively similar to those at L = 0.5, but quantitatively different; that is, the bottom face produces maximum heat transfer at the lowest L = 0.1. In this bottom face, the Nusselt number is almost constant in the major portion since the gap flow is found minimum at L = 0.1 (Fig. 6(b)). Higher Nu-value on this face is due to the fact that the bottom face is very close to the cold plane wall. As a result, the distance between T_W and T_0 becomes minimum, and the conductive heat transfer through the plane wall takes place (Fig. 7(b)). Moreover, at this L = 0.1, the maximum variation

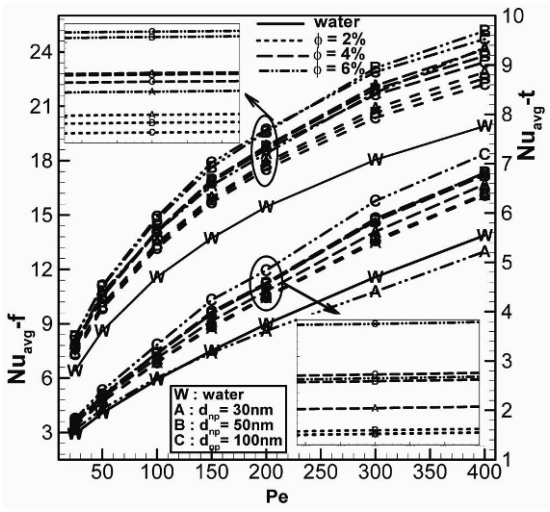

(a)

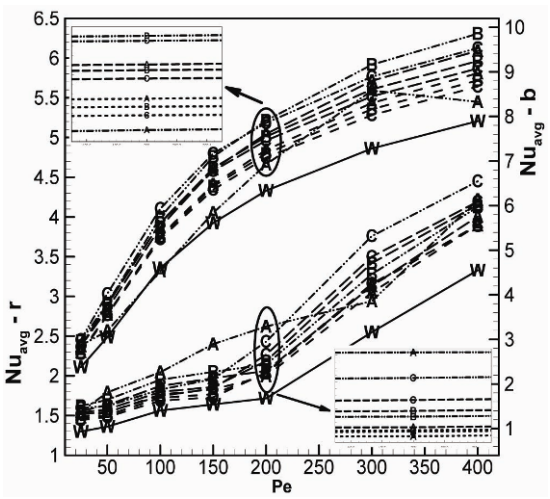

(b)

Fig. 8. Face average Nusselt number (Nu_{avg}) along the surfaces of the cylinder as a function of *Pe*, φ and d_{np} for H_2O-Al_2O_3 nanofluid. Here subscripts *f, r, t* and *b* stand for front, rear, top and bottom, respectively.

in *Nu*-distribution is observed on the face (Rear) where the *Nu*-variation is minimum at other *L*. For $L \geq 0.5$, the *Nu* at each point on the surfaces increases with *L*, because of the higher incident velocity.

Face-averaged Nusselt numbers (Front face: Nu_{avg}-*f*, rear face: Nu_{avg}-*r*, top face: Nu_{avg}-*t* and bottom face: Nu_{avg}-*b*) as a function of *Pe,* φ and d_{np} are presented in Fig. 8. At any particular parameter value, the front face shows maximum heat transfer, while the rear face dissipates minimum heat transfer, among all faces. Though the flow around the cylinder is asymmetric, heat transfers from the bottom and top faces are almost equal for $Pe \geq 100$. At a lower *Pe* (< 100), the bottom face shows slightly lower heat transfer than the top face. As high as *Pe,* the *Re* becomes higher, which leads to accelerating the gap flow. Nu_{avg}-*f* almost linearly increases with *Pe*, while the effect of *Pe* on Nu_{avg}-*r* is more at a higher

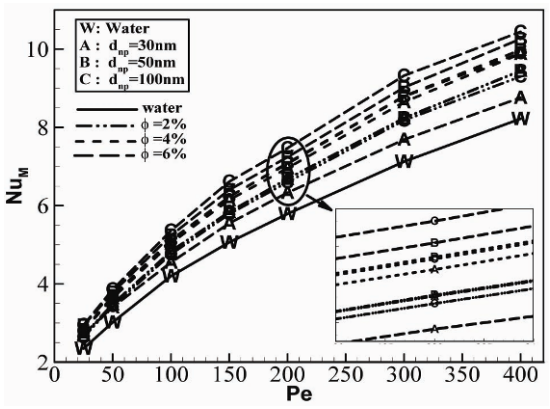

(a)

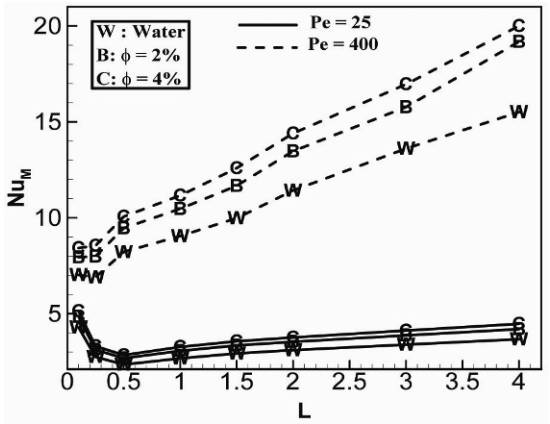

(b)

Fig. 9. Mean Nusselt number (Nu_M) across the cylinder as a function of (a) *Pe* for different φ and d_{np}; (b) *L* for *Pe* = 25, 400, φ = 0, 2, 4 % at d_{np} = 50 nm.

Pe than at a lower *Pe*. The curves along the top face are similar to their respective curves along the bottom face. Note that the addition of nanoparticles does not necessarily increase the heat transfer from all faces. Here, the *Nu* from the front face for d_{np} = 30 nm and φ = 6 % is found to be less than that for the pure water case. The speed of the incident cold fluid on the front face is the major constituent of the total heat transfer from this face. Here, for d_{np} = 30 nm and φ = 6 % (*Re* = 21.55*)* the fluid velocity is lower than that of pure water (*Re* = 65.15) at *Pe* = 400. In fact, the value of *Re* for the curve corresponding to d_{np} = 100 nm with φ = 6 % is 88.4. Nevertheless, the overall heat transfer (Nu_M) from the cylinder is found to be more for nanofluids (Fig. 9). The curves corresponding to highest ϕ lie above the respective curves for the lower ϕ (Fig. 9).

Effects of φ, d_{np} and *Pe* on Nu_M are presented in Fig. 9(a), while Fig. 9(b) presents Nu_M as a function of *L* at *Pe* = 25 and 400 for H_2O-Al_2O_3. As seen in Fig. 9(a), all the Nu_M curves are qualitatively similar, not crossing each other. For a particular combination of φ and d_{np}, *i.e.*, for a fixed value of *Pr*, the Nu_M increases with *Pe*. Here, increase of *Pe* is due to the increase in *Re* for a particular curve. Therefore, the increment in

Nu_M due to *Pe* is attributed to the increased intensity of the incident velocity. Effects of d_{np} and φ on the heat transfer rate are found to be more at a higher *Pe* (*i.e*), at a higher *Re*. The case with d_{np} = 100 nm and φ = 6 % maximizes the heat transfer enhancement from the cylinder at all *Pe* since the value of *Re* is more at all *Pe* for this case compared to other cases. At higher *Re*, Brownian motion has an important role in heat transfer (Ebrahimnia-Bajestan et al. [7]). With the increase of φ, Nu_M increases at all *Pe* for d_{np} = 50 nm and 100 nm. As noted in Fig. 9(a), only for the case of d_{np} = 30 *nm*, Nu_M is found to decrease with increase of φ from 4 to 6 %. Though there is a large increase in μ_{nf} than the increase in κ_{nf} at φ = 6 % and d_{np} = 30 nm (Fig. 2), all nanofluids considered here can be used as coolants compared to the base fluid. The increment in Nu_M (from the value of its base fluid case) is about 6.57 % to 29.02 % depending on the values of d_{np}, φ and *Pe*. Therefore, the increased number of nanoparticles in the base fluid where the κ_{nf} is more effective (Than μ_{nf}) on heat transfer is responsible for the improved values of Nu_M. Again at φ = 6 % a reverse trend in Nu_M with d_{np} is observed since *Pr* decreases with the increase of d_{np} at much faster rate compared to φ=2 % and 4 % cases. Note that the present results (Based on variations of *Pe*, φ and d_{np}) are analogous to Ebrahimnia-Bajestan et al. [7]. To discuss the effect of nano-materials on the heat transfer, a similar effort was made for the case of H_2O-*CuO*, not presented here. The Nu_M follows similar trends of its respective curve plotted in Fig. 9(a) as the *Pe* increases. However, the presence of the *CuO* nanoparticle in water is slightly more pronounced on the heat transfer from the cylinder compared to that of Al_2O_3 nanoparticle presence. For example, at *Pe* = 200, the increment in Nu_M of H_2O-*CuO* (from the value of base fluid water case) is about 7.18 % to 21.24 %, while this value for Nu_M of H_2O-Al_2O_3 is about 6.57 % to 20.20 %. A similar effect on the Nu_M is also observed due to the variations of d_{np} and φ. As depicted in Fig. 9(b), the Nu_M variation is not uniform with *L*, that is, with the increase of *L*, the Nu_M starts to decline and becomes minimum at *L* = 0.5 and 0.25 for *Pe* = 25 and 400, respectively, and thereafter increases with *L*. However, for the case of *Pe* = 25, Nu_M could not reach the value as the lowest *L* = 0.1 even at a gap height *L* = 4.0, because at this lower *Pe*, the value of *Re* is so small (Falls in (4,4.65)) that the change of the gap height would not give noticeable variation in the incident velocity. This variation of Nu_M with *L* can be observed at higher *Pe* (i.e., *Re*) and the heat transfer is remarkably enhanced at higher *L*.

An explicit form of functional dependency of Nu_M on *Pe* and *L* is presented using the least square method in Table 4 for H_2O-Al_2O_3 nanofluid with d_{np} = 50 nm. As seen in Table 4, R^2 is very close to 1.0 while *RSS* is less, indicating that the proposed relations (Especially $Nu_M = Nu_M(Pe)$) are the best fitted relations. It is reconfirmed in the equations $Nu_M = Nu_M(Pe)$ that the Nu_M increases with *Pe*, but the increasing/decreasing of $Nu_M = Nu_M(L)$ is dependent on *Pe*. When the equations as well as their coefficients are compared to each other, all the observations made so far on the dependency of Nu_M on *Pe*, ϕ and *L* (Based on its graphical representation) are consistent with these explicit functional forms of Nu_M.

Table 4. Explicit form of functional dependency of Nu_M on *Pe* and *L* for H_2O-Al_2O_3 nanofluid with d_{np} = 50 nm. Residual sum of squares (RSS) and coefficient of determination (R^2) are written in first bracket against each relation.

ϕ	$Nu_M = Nu_M(Pe)$
2 %	$Nu_M = (1.153Pe + 1.579)^{1/2}$ (0.0047, 0.9998)
4 %	$Nu_M = (1.239Pe + 1.734)^{1/2}$ (0.0027, 0.9999)
6 %	$Nu_M = (1.571Pe + 1.924)^{1/2}$ (0.009, 0.9997)
Pe	$Nu_M = N_M(L)$
25	$Nu_M = 3.599L^{-0.0141/L}$ (2.274, 0.4089)
400	$Nu_M = 2.966L + 8.189$ (0.4010, 0.9966)

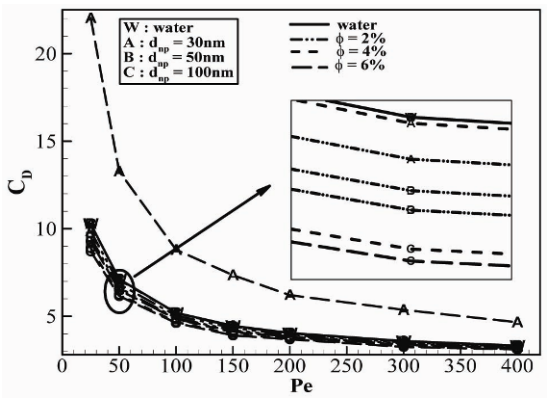

(a)

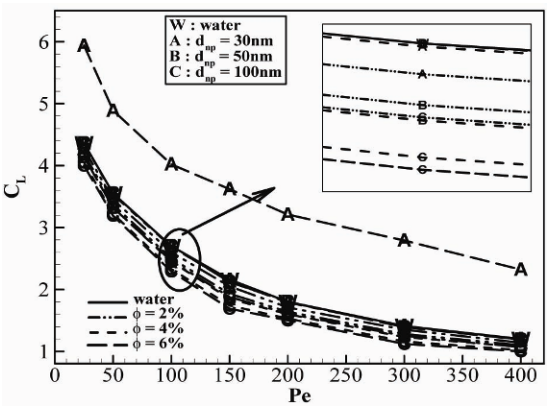

(b)

Fig. 10. Variation of (a) C_D; (b) C_L with *Pe* for H_2O-Al_2O_3 nanofluid at different d_{np} and φ.

The dependence of the hydrodynamic coefficients (Drag coefficient C_D and lift coefficient C_L) on *Pe*, d_{np} and φ was analyzed with the help of Fig. 10(a) (for C_D) and Fig. 10(b) (for C_L). The C_D at different d_{np} and φ shows qualitatively similar behavior with a change in *Pe,* monotonically decreasing with the increase of *Pe*. The C_D dependence on *Pe* becomes weaker at a higher range of *Pe*. Maiti [23] reported that C_D decreases with the increase of *Re* at a lower range of *Re* ($\leq$ 200). Here the maximum value of *Re* among all the cases

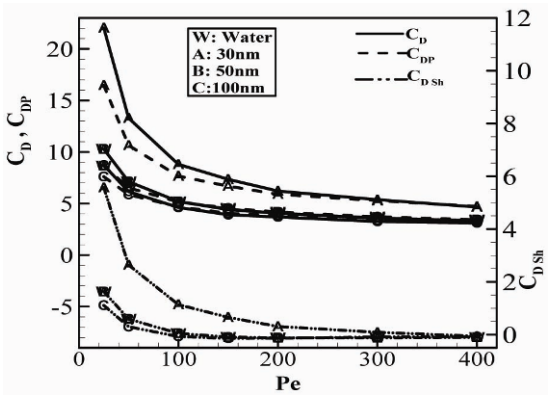

(a)

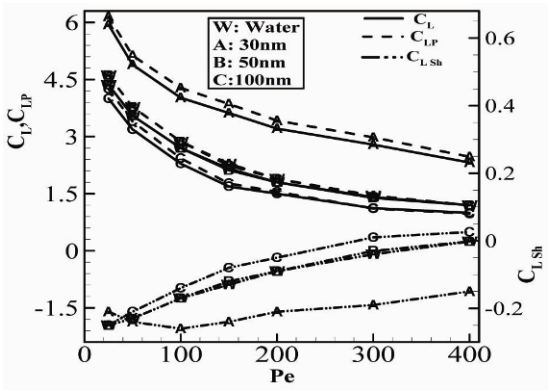

(b)

Fig. 11. (a) Comparison of drag coefficients (C_D) with their counterpart due to pressure (C_{DP}) and due to shear ($C_{D\,Sh}$); (b) comparison of lift coefficient (C_L) with their counterpart due to pressure (C_{LP}) and due to shear ($C_{L\,Sh}$) at different *Pe* for H_2O-Al_2O_3 nanofluid with $\varphi = 6$ %.

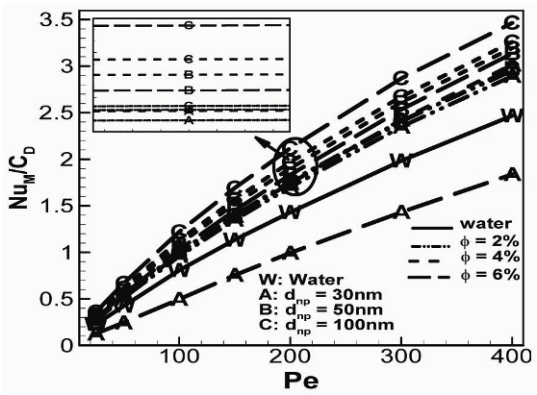

(a)

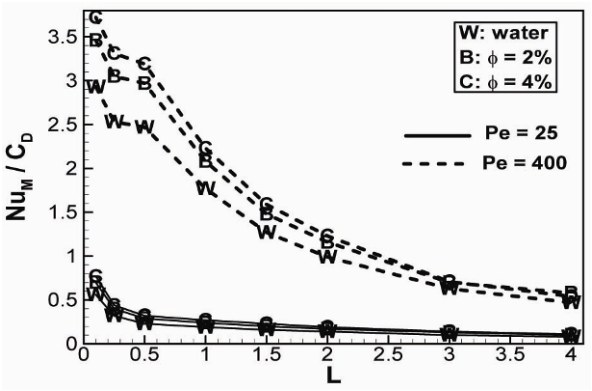

(b)

Fig. 12. Ratio of Nusselt number to drag coefficient (Nu_M/C_D) of the cylinder for different values of (a) *Pe*, ϕ and d_{np}, for $L = 0.5$; (b) *L* with *Pe* = 25 and 400; $\phi = 0, 2, 4$ %.

is around 100. Note that ϕ have some effect on C_D only at the lower range of *Pe*. Also, the curve corresponding to φ = 6 % with d_{np} = 30 nm shows much more higher value of C_D to the cylinder at all *Pe*. As in this case *Pr* = 18.85, the *Re* registers much lower value where viscous effect becomes more significant. All C_L curves show qualitatively similar behavior with changing *Pe*. Like C_D, C_L also decreases with the increase of *Pe*, but the variation is found continuous over the whole range of *Pe*. Moreover, the effects of φ and d_{np} on C_L are pronounced over the whole range of *Pe*. Essentially the curve corresponding to d_{np} = 30 nm (6 %) in Fig. 10(b) also distinctly appears among all other curves and lift coefficient of the cylinder becomes much more for the case of φ =6 % with d_{np} = 30 nm. For fixed nanofluid (for given material, φ and d_{np}), the present observation on effect of *Re* (Due to variation of *Pe*) on C_L is analogous to that of Maiti [23]. Apparently, hydrodynamic forces for H_2O-*CuO* nanofluid are found comparable to the respective force for H_2O-Al_2O_3 nanofluid at each value of d_{np} and φ, therefore not presented here. Also, the variations of hydrodynamic forces with the gap height for the present case of nanofluid are qualitatively similar to those (C_D increases uniformly with *L* while C_L is not uniform with *L*) for the case of without nanofluid reported in the previous study (Maiti [33]), consequently it is avoided here. The role of viscosity on the hydrodynamic forces at φ = 6 % is discussed by presenting the drag and lift coefficients due to pressure and shear (Figs. 11(a) and (b)) for the case of H_2O-Al_2O_3 and d_{np} = 30, 50 and 100 nm. Values for the base fluid are also presented. As seen in Figs. 11(a) and (b), the solid curve appears close to the respective dashed curve, indicating that the pressure force is the major constituent of the overall hydrodynamic forces. Curves corresponding to d_{np} = 30 nm appear distinctly, and it is immediately evident that viscous forces for both lift and drag coefficients have an appreciable contribution to the total hydrodynamics forces at lower *Pe*, remarkably for d_{np} = 30 nm.

To assess the heat transfer enhancement of the heated cylinder together with its drag coefficient reduction/increment due to the variation of *Pe* and *L* in nanofluid flow, Fig. 12 is presented for Nu_M/C_D against *Pe* (Fig. 12(a)) and *L* (Fig. 12(b)). Eventually, the ratio increases with *Pe* in Fig. 12(a) since Nu_M increases while C_D decreases with the increase of *Pe*. As seen in Fig. 12(a), the curve for d_{np} = 100 nm with φ = 6 % appears at the top of all curves, while the curve for d_{np} = 30 nm with φ = 6 % appears at the bottom, even below the curve-*W*. Unlike Fig. 12(a), the ratio decreases with *L* at both

Pe, and at a lower *Pe* the variation becomes negligible at higher *L* (> 1.5). These results indicate that the rate at which the heat transfer enhancement occurs with *L* is less than that of drag coefficient increment. It also suggests that placing the cylinder sufficiently close to the plane wall is beneficial in terms of the heat transfer enhancement along with minimum drag coefficient. It may be noted that the ratio is more for nanofluids case in comparison to clear fluid case at both *Pe*.

4. Conclusion

The nanofluid (H_2O-Al_2O_3/CuO) flow over a heated square cylinder placed near a cold wall was numerically studied under the incident of Couette flow at the inlet. It was observed that front stagnation point shifts very close to the bottom of the front face for the case of φ = 6 % with d_{np} = 30 nm and moves towards the bottom side as *L* increases. In-spite of asymmetry in the flow around the cylinder (Due to incident shear flow and presence of the wall), heat transfers from the bottom and top faces are reported almost equal for $Pe \geq 100$ at $L = 0.5$. Interestingly, addition of nanoparticles did not necessarily increase the heat transfer from all faces. At lower *Pe* = 25, the maximum heat transfer was from the bottom face (Among all faces) at the lowest $L = 0.1$. Nusselt number (Nu_M) increased with the increase of *Pe*. Except for d_{np} = 30 nm (and φ = 6 %), Nu_M increased (and decreased) with an increase of φ (and d_{np}) at all *Pe*. Surprisingly only for the case of d_{np} = 30 nm, Nu_M was found to decrease with an increase in φ from 4-6 % due to a sudden jump in *Pr* from Pr = 6.086 to 18.85 with φ changing from 4-6 %. Overall, though there was a larger increase in μ_{nf} than that in κ_{nf} at φ = 6 % and d_{np} = 30 nm, all nanofluids considered here can be used as coolants compared to the base fluid. The increment in Nu_M was about 6.57 % to 29.02 % depending on the values of d_{np}, φ and *Pe* at $L = 0.5$. The heat transfer enhancement from the cylinder was slightly more for *CuO* compared to Al_2O_3. Effects of diameter and concentration of nanoparticles on the heat transfer were observed more at a higher *Pe*. At a lower *Pe* = 25, the maximum Nu_M was found at the lowest *L* examined, while at a higher *Pe* = 400, Nu_M increased with *L*. Observations based on the graphical representation of dependencies of Nu_M on *Pe* (at $L = 0.5$) and *L* (at *Pe* = 25 and 400) were reconfirmed by presenting their explicit functional form $Nu_M = Nu_M(Pe)$ and $Nu_M = Nu_M(L)$. C_D and C_L both decreased with the increase of Pe. Essentially, C_L and C_D curves corresponding to φ =6 % with d_{np} = 30 nm distinctly appeared from all other curves, and C_D and C_L both registered much higher values. The ratio Nu_M/C_D increased with *Pe*, while decreased with *L* increased, and was more at each *L* for the nanofluid case in comparison to clear fluid case at both *Pe*.

An anomalous behavior of the effective viscosity of nanofluid (μ_{nf}) (Consequently of hydrodynamics and heat transfer characteristics) with φ within the defined range of φ for the case of d_{np} = 30 nm suggests that the mathematical restriction (Provided by Masoumi et al. [32]) on the range of φ is not sufficient. In addition, one needs to check the continuity in variation of μ_{nf} with φ for a particular d_{np}, and then the maximum value of φ should be taken accordingly. The present numerical experiment was conducted on the physical property of nanofluid at room temperature. It is plausible that temperature has an important role on the κ_{nf} and μ_{nf} of nanofluid, and hence on heat transfer enhancement rate. This is one possible future work, which will be taken care in our next study.

Acknowledgment

Maiti acknowledges the financial assistance of DST (INDIA) (Sanction No. SR/S4/MS/820/13 dated 07.05.2015) and CTS, IIT, Kharagpur, India. Alam wishes to acknowledge support given to him from the Research Grant Council of Shenzen Government through grant JCYJ2016053119144 2288.

References

[1] R. J. Yang and L. M. Fu, Thermal and flow analysis of a heated electronic component, *Int. J. Heat Mass Transf.,* 44 (12) (2001) 2261-2275.

[2] S. U. S Choi, Enhancing thermal conductivity of fluid with nanoparticles in development and applications of non-Newtonian flows, *ASME*, 231 (1995) 99-105.

[3] C. T. Nguyen, G. Roy, C. Gauthier and N. Galanis, Heat transfer enhancement using Al_2O_3-water nanofluid for an electronic liquid cooling system, *Appl. Therm. Eng*., 27 (2007) 1501-1506.

[4] W. H. Azmi, K. A. Hamid, N. A. Usri, R. Mamat and K. V. Sharma, Heat transfer augmentation of ethylene glycol: water nanofluids and applications—A review, *Int. Commun. Heat Mass Transf.,* 75 (2016) 13-23.

[5] S. Kakaç and A. Pramuanjaroenkij, Review of convective heat transfer enhancement with nanofluids, *Int. J. Heat Mass Transf.,* 52 (13) (2009) 3187-3196.

[6] S. M. S. Murshed, K. C. Leong and C. Yang, Investigations of thermal conductivity and viscosity of nanofluids, *Int. J. Therm. Sci.,* 47 (5) (2008) 560-568.

[7] B. E. Ebrahimnia, H. Niazmand, W. Duangthongsuk, S. Wongwises and M. Renksizulut, Numerical investigation of effective parameters in convective heat transfer of nanofluids flowing under laminar flow regime, *Int J. Heat Mass Transf.,* 54 (19-20) (2011) 4376-4388.

[8] A. Sharma and V. Eswaran, Heat and fluid flow across a square cylinder in the two-dimensional laminar flow regime, *Numer. Heat Transf. Part A,* 45 (2004) 247-269.

[9] S. Bhattacharya, D. K. Maiti and S. Dhinakaran, Influence of buoyancy on vortex shedding and heat transfer from a square cylinder in wall proximity, *Numer. Heat Transf. Part A*, 50 (2006) 585-606.

[10] S. Dhinakaran, Heat transport from a bluff body near a moving wall at Re= 100, *Int. J. Heat Mass Transf.,* 54 (25)

(2011) 5444-5458.
[11] S. H. Zeinali, S. G. Etemad and M. N. Esfahany, Experimental investigation of oxide nanofluids laminar flow convective heat transfer, *Int. Commun. Heat Mass Transf.,* 33 (4) (2006) 529-535.
[12] M. S. Valipour, R. Masoodi, S. Rashidi, M. Bovand and M. Mirhosseini, A numerical study on convection around a square cylinder using Al_2O_3-H_2O nanofluid, *Int. J. Therm. Sci*., 18 (4) (2014) 1305-1314.
[13] M. Bovand, S. Rashidi and J. A. Esfahani, Enhancement of heat transfer by nanofluids and orientations of the equilateral triangular obstacle, *Energy Conv. Mngmt*., 97 (2015) 212-223.
[14] M. Sheikholeslami, M. Gorji-Bandpy and K. Vajravelu, Lattice Boltzmann simulation of magnetohydrodynamic natural convection heat transfer of Al_2O_3-water nanofluid in a horizontal cylindrical enclosure with an inner triangular cylinder, *Int. J. Heat Mass Transf.,* 80 (2015) 16-25.
[15] M. R. Salimpour and A. D. Parizi, Convective heat transfer of nanofluid flow through conduits with different cross-sectional shapes, *J. Mech. Sci. Eng*., 29 (2) (2015) 707-713.
[16] H. Heidary and M. J. Kermani, Heat transfer enhancement in a channel with block(s) effect and utilizing nanofluid, *Int. J. Therm. Sci.,* 57 (2012) 163-171.
[17] M. Azimi and R. Riazi, MHD copper-water nanofluid flow and heat transfer through convergent-divergent channel, *J. Mech. Sci. Eng.,* 30 (10) (2016) 4679-4686.
[18] F. V. Etminan, E. Ebrahimnia, H. Niazmand and S. Wongwises, Unconfined laminar nanofluid flow and heat transfer around a square cylinder, *Int. J. Heat Mass Transf.,* 55 (2012) 1475-1485.
[19] S. Sarkar and S. Ganguly, Analysis of entropy generation during mixed convective heat transfer of nanofluids past a square cylinder in vertically upward flow, *J. Heat Transf.,* 134 (2012) 122501.
[20] Z. Alloui, J. Guiet, P. Vasseur and M. Reggio, Natural convection of nanofluids in a shallow rectangular enclosure heated from the side, *Canadian J. Chem. Eng.,* 90 (1) (2012) 69-78.
[21] A. Noghrehabadi, A. S. Behbahan and I. Pop, Thermophoresis and brownian effects on natural convection of nanofluids in a square enclosure with two pairs of heat source/sink, *Int. J. Num. Meth. Heat Fluid Flow,* 25 (5) (2015) 1030-1046.
[22] S. Malik and A. K. Nayak, Buoyancy driven heat transfer in nanofluids due to wall mounted heat source, *Alex Eng. Journal,* 55 (2016) 797-810.
[23] D. K. Maiti, Dependence of flow characteristics of rectangular cylinders near a wall on the incident velocity, *Acta Mechanica,* 222 (2011) 273-286.
[24] M. Akbari, N. Galanis and A. Behzadmehr, Comparative analysis of single and two-phase models for CFD studies of nanofluid heat transfer, *Int. J. Therm. Sci.,* 50 (8) (2011) 1343-1354.
[25] M. Corcione, M. Cianfrini, E. Habib and A. Quintino, Optimization of free convection heat transfer from vertical plates using nanofluids, *J. Heat Transf.,* 134 (4) (2012) 042501.
[26] S. M. Vanaki, P. Ganesan and H. A. Mohammed, Numerical study of convective heat transfer of nanofluids: A review, *Renew. Sustain. Energy Reviews,* 54 (2016) 1212-1239.
[27] B. C. Pak and Y. I. Cho, Hydrodynamic and heat transfer study of dispersed fluids with submicron metallic oxide particles, *Exp. Heat Transf.,* 11 (2) (1998) 151-170.
[28] Y. Xuan and W. Roetzel, Conceptions for heat transfer correlation of nanofluids, *Int. J. Heat Mass Transf.,* 43 (19) (2000) 3701-3707.
[29] J. Koo and C. Kleinstreuer, A new thermal conductivity model for nanofluids, *J. Nanopart Res.,* 6 (6) (2004) 577-588.
[30] R. S. Vajjha and D. K. Das, Experimental determination of thermal conductivity of three nanofluids and development of new correlations, *Int. J. Heat Mass Transfer.,* 52 (21-22) (2009) 4675-4682.
[31] D. Kim, Y. Kwon, Y. Cho, C. Li, S. Cheong, Y. Hwang, J. Lee, D. Hong and S. Moon, Convective heat transfer characteristics of nanofluids under laminar and turbulent flow conditions, *Curr. Appl. Phys.,* 9 (2) (2009) e119-e123.
[32] N. Masoumi, N. Sohrabi and A. Behzadmehr, A new model for calculating the effective viscosity of nanofluids, *J. Phys. D. Appl. Phys*., 42 (5) (2009) 055501.
[33] D. K. Maiti, Aerodynamic characteristics of rectangular cylinders near a wall, *J. Ocean Eng.,* 54 (2012) 251-260.
[34] S. Bhattacharya and D. K. Maiti, Shear flow past a square cylinder near a wall, *Int. J. Eng. Sci.,* 42 (2004) 2119-2134.

Swati Sharma received her M.S. in Applied Mathematics from University of Delhi, Delhi, India in 2009. She is currently a Ph.D. candidate in Mathematics, BITS PILANI, Pilani Campus, Rajasthan, India. Her research area is computational fluid dynamics.

Dilip K. Maiti received his Ph.D. in Mathematics from IIT Kharagpur, India in 2005. He is currently an Associate Professor and Head of Applied Mathematics with Oceanology and Computer Programming, Vidyasagar University, India. His research interests include nanofluid heat transfer over cylinder/s under the incident of Couette-Poiseuille flow, heat and mass transfer in cavity, micro channel Flow.